

Little Red Dots as the Very First Activity of Black Hole Growth

KOHEI INAYOSHI ¹

¹*Kavli Institute for Astronomy and Astrophysics, Peking University, Beijing 100871, China*

ABSTRACT

The James Webb Space Telescope has detected massive black holes (BHs) with masses of $\sim 10^{6-8} M_{\odot}$ within the first billion years of the universe. One of the remarkable findings is the identification of “Little Red Dots” (LRDs), a unique class of active galactic nuclei (AGNs) with distinct characteristics representing a key phase in the formation and growth of early BHs. Here, we analyze the occurrence rate of LRDs, which emerge around redshifts $z \sim 6-8$ and sharply decline at $z < 4$. We find that this trend follows a log-normal distribution, commonly observed in phenomena driven by stochastic and random factors. We propose a hypothesis that the first one or two AGN events associated with newly-formed seed BHs are observed as LRDs and their unique features fade in the subsequent episodes. This naturally explains the cosmic evolution of AGN abundance over $0 < z < 5$, which follows $\propto (1+z)^{-5/2}$ due to the cumulative effect of recurring AGN activity. The unique characteristics of LRDs are likely linked to the dense gas environments around the seed BHs, which create strong absorption features in the broad-line emission and enable super-Eddington accretion bursts, ultimately yielding the observed overmassive nature of BHs compared to the local relationship.

Keywords: Galaxy formation (595); High-redshift galaxies (734); Quasars (1319); Supermassive black holes (1663)

1. INTRODUCTION

The James Webb Space Telescope (JWST) has revolutionized extragalactic research, uncovering low-luminosity AGNs at high redshifts of $z > 4-7$ powered by accreting BHs with masses of $\sim 10^{6-8} M_{\odot}$ (e.g., Onoue et al. 2023; Kocevski et al. 2023; Harikane et al. 2023; Maiolino et al. 2023; Taylor et al. 2024). Among these ground-breaking discoveries, the identification of “Little Red Dots” (LRDs) stand out as particularly remarkable. LRDs are extremely compact objects (< 100 pc) characterized by broad emission lines on red continuum spectra, indicating the presence of dust-obscured AGNs (e.g., Matthee et al. 2024; Greene et al. 2024; Labbe et al. 2023). Their cosmic abundance is several orders of magnitude higher than that of bright quasars, allowing them to be detectable even within JWST’s narrow field of view (Kokorev et al. 2024; Akins et al. 2024; Kocevski et al. 2024). These objects show BH-to-galaxy mass ratios far above the empirical values observed in the nearby universe (e.g., Kormendy

& Ho 2013; Reines & Volonteri 2015), suggesting that they preserve crucial information on the formation of seed BHs and their early rapid growth phases.

Despite their significance, key questions about the spectral nature of LRDs arise from multi-wavelength observations (e.g., Kocevski et al. 2024; Greene et al. 2024; Juodžbalis et al. 2024; Pérez-González et al. 2024; Maiolino et al. 2024; Wang et al. 2024a,b): (1) the prominent absorption feature in broad Balmer emission lines, (2) the deficit of hot dust emission, (3) the “v-shape” SED in the rest-frame UV-optical range, and (4) the absence of X-ray detections. These characteristics indicate that LRDs might represent a unique phase of AGN activity in their formation, and a potential contribution from super-Eddington accretion (Inayoshi et al. 2020; Volonteri et al. 2021, references therein).

2. COSMIC EVOLUTION OF LRD NUMBERS

To date, more than 300 LRDs have been identified through JWST survey programs, using photometric color selection techniques. We adopt a sample of 341 LRDs spanning over $z \sim 2-11$, compiled from the CEERS, PRIMER, JADES, UNCOVER and NGDEEP surveys (Kocevski et al. 2024). These LRDs were selected using a spectral slope fitting technique, which em-

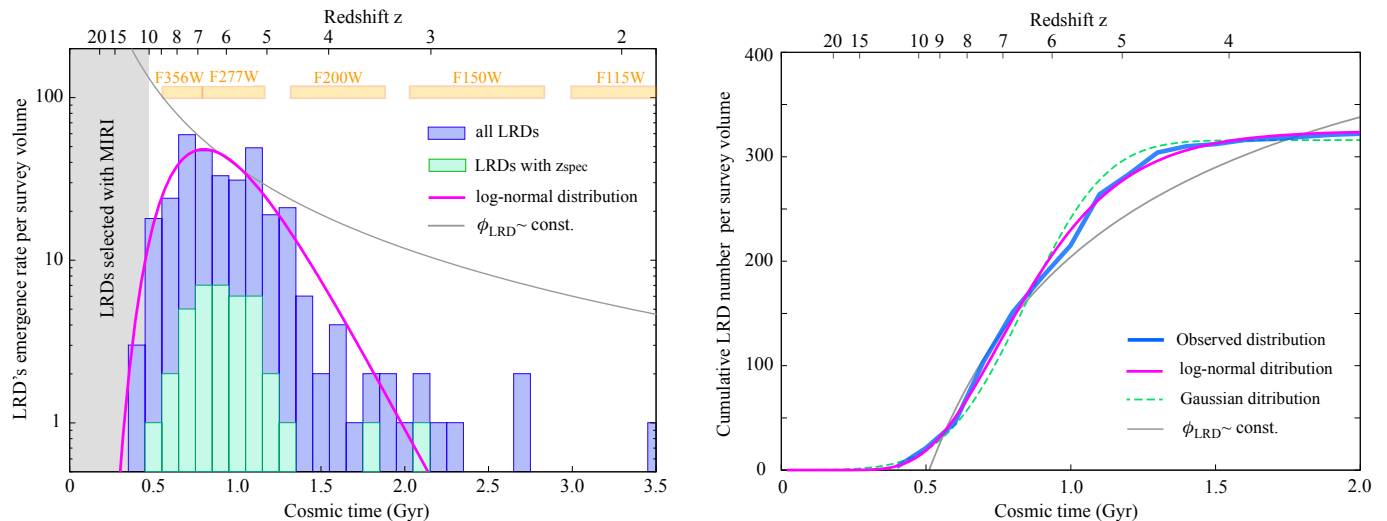


Figure 1. *Left:* The occurrence rate of LRDs as a function of cosmic time (bottom x -axis) and redshift (top x -axis). The histogram, based on the data from Kocevski et al. (2024), shows 341 photometrically-selected LRDs (blue), including 39 with spectroscopically-confirmed redshifts (green). The colored bars indicate the redshift range where the 4000 \AA break falls within the bandpass of each wide-band filter. The photometric selection of $z > 9$ LRDs becomes incomplete (gray shaded region). The magenta curve represents the best-fit function with a log-normal distribution, while the gray curve shows the case with constant abundance in unit comoving volume for reference. *Right:* The cumulative number distribution of the observed LRD number (blue). The best-fit result obtained using a log-normal distribution is shown, along with a Gaussian distribution yielding a similarly good fit.

employs shifting bandpasses to sample the same rest-frame emission both blueward and redward of the 4000 \AA break, and enables a self-consistent search for AGN candidates with red optical and blue UV colors over a wide range of redshifts (see also Hainline et al. 2025).

In the left panel of Figure 1, we present the occurrence rate of the LRD sample as a function of cosmic time (bottom x -axis) and redshift (top x -axis). The histogram shows 341 photometrically-selected LRDs (blue), including 39 with spectroscopically-confirmed redshift. The colored bars indicate the redshift range where the 4000 \AA break falls within the bandpass of each wide-band filter. These LRDs with unique v-shape spectra and compact morphology emerge at $z \sim 8$, but the number begins to decline at $z \lesssim 6$, and experience a rapid drop at $z \sim 4$ (Kocevski et al. 2024). For $z > 8$, the turnover wavelength enters the F356W band, while red optical continua are observed only in F444W (and F410M, if available). As a result, the selection of $z > 9$ LRDs becomes incomplete and thus the number might drop toward higher redshifts. On the low-redshift side ($z < 4$), the number of LRD detections rapidly decreases, even though the available NIRCcam bands are capable of capturing the 4000 \AA break. It is worth noting that the histogram distributions of the total LRD sample and the subset with spectroscopic redshifts show similar shapes without significant skewness. This suggests that photometric redshift measurements provide

a reliable estimate of their true values for these LRD samples. For comparison, we consider a scenario where the comoving number density of LRDs remains constant over time, yielding a reference evolution for the occurrence rate: $dN/dt = \phi \cdot (dV_c/dz)(dz/dt) \propto t^{-5/3}$, or equivalently $\propto (1+z)^{5/2}$ (gray curve). The observed decline in the LRD occurrence rate, however, deviates significantly from the reference evolution.

This implies that LRD activity is not a process that repeats continuously over cosmic time, but instead occurs sporadically due to complex and random factors. In many natural systems (e.g., earthquakes and astronomical phenomena such as gamma-ray bursts and fast radio bursts), the waiting time between successive events follows a log-normal distribution (e.g., Li & Fenimore 1996; Ellsworth et al. 1999; Kirsten et al. 2024), reflecting the stochastic nature of these events. Inspired by these analogies, we employ the standard χ^2 minimization technique to fit the observed data using a log-normal distribution defined as

$$\frac{dN}{dt} = \frac{N_0}{\sqrt{2\pi}\sigma_0 t} \exp\left[-\frac{\{\ln(t/t_0)\}^2}{2\sigma_0^2}\right] \quad (1)$$

From the fitting procedure, we find the best-fit parameters: $t_0 = 888 \pm 30 \text{ Myr}$ and $\sigma_0 = 0.326 \pm 0.0341$ with a time bin of $\Delta t = 100 \text{ Myr}$ (magenta curve). Importantly, the log-normal fit remains robust even when the histogram is restricted to LRDs with UV absolute mag-

nitudes, $M_{UV} < -18$ mag, where detection is not significantly affected by flux limits. This strengthens the validity of our argument, indicating that the observed trend is intrinsic to LRDs rather than a selection effect (see more details in Appendix A).

In the right panel of Figure 1, we show the cumulative number distribution of LRDs. For $t > 1.3$ Gyr, the distribution flattens due to the sharp decline in the number of sources. For comparison, we overlay three curves representing different fitted distribution functions for the occurrence rate: a log-normal distribution (magenta), a Gaussian distribution (green), and a power-law form with $dN/dt \propto t^{-5/3}$ (gray), which assumes a constant ϕ_{LRD} . The log-normal distribution provides our best-fit model with $t_0 = 837 \pm 6$ Myr and $\sigma_0 = 0.331 \pm 0.0105$. These values are in good agreement with the previous fitting results for the occurrence rate¹. The Gaussian model yields a slightly worse fit, as the function form fails to capture the asymmetric feature of the distribution (we note that incompleteness of LRD detections at $z > 9$ might further influence the goodness of fit for the Gaussian model). The power-law model does not explain the flattening of the cumulative distribution. Even when the power-law index is treated as a free parameter, the best-fitting function ($dN/dt \propto t^{-2.59}$) still does not match the observed trend well. Such a steep decline cannot be only attributed to the loss of LRD features, particularly their compact morphology, due to mergers with normal galaxies (see Appendix B), though merger may play a partial role in their disappearance.

3. DISCUSSION

Based on our finding that the occurrence rate of LRDs follows a log-normal distribution, we propose a hypothesis for the origin of LRDs: the first one or two AGN events associated with a newly-formed seed BH are observed as LRDs due to the unique characteristics of the surrounding environment. After these initial accretion episodes, the LRD features fade and the objects transition into normal AGNs.

In this scenario, LRDs represent the earliest phase of AGN activity from newly-born BH seeds with $\sim 10^{4-5} M_\odot$, which are likely embedded in dense gas environments (e.g., Bromm & Loeb 2003; Begelman et al. 2006; Shang et al. 2010) with abundances of $\sim 10^{-5} - 10^{-4} \text{ Mpc}^{-3}$, corresponding to those of atomic-cooling halos in overdense regions where intense Lyman-

Werner radiation and/or violent halo mergers enhance the possibility of BH seeding through suppression of H_2 formation and cooling (e.g., Valiante et al. 2016; Li et al. 2021, 2023; Trinca et al. 2022). This dense gas leads to strong absorption features on top of the broad Balmer emission lines, which is one of the key spectral signatures for LRDs (Matthee et al. 2024; Juodžbalis et al. 2024; Ji et al. 2025). Furthermore, if the gas surrounding the seed BH accretes at super-Eddington rates, this would naturally explain the observed X-ray weakness and weak (but observable) variability of LRDs (Madau & Haardt 2024; Inayoshi et al. 2024). When the BH grows rapidly at a rate with an Eddington ratio of $\lambda_{\text{Edd}} \sim O(10)$, the e -folding time of BH growth is $t_{\text{grow}} \simeq 1.5 \text{ Myr} (\lambda_{\text{Edd}}/30)^{-1}$. This implies that the seed BH can reach a mass of $10^7 M_\odot$ within just one or two accretion episodes, each lasting several Myrs (e.g., Inayoshi et al. 2022). Once the BH grow in mass substantially, super-Eddington accretion becomes unsustainable due to a reduced mass supply from the galaxy environment (Hu et al. 2022; Scoggins & Haiman 2024). As a result, the BH transitions from the early super-Eddington accretion phase to a more typical AGN phase, after making the BHs largely overmassive compared to the BH-to-galaxy mass ratio measured in the nearby universe (e.g., Harikane et al. 2023; Maiolino et al. 2023; Kocevski et al. 2024; Chen et al. 2024).

Assuming the physical processes driving both LRDs and normal AGNs are essentially the same, and the time interval between each individual event follows a similar statistical distribution, the cosmic evolution of AGN abundances should evolve in a similar fashion for LRDs. However, observations reveal that while LRDs show a rapid decline in occurrence rate, the occurrence rate of normal AGNs remains nearly constant down to low redshifts (Ueda et al. 2014; Delvecchio et al. 2014; Pouliaxis et al. 2024). This discrepancy suggests that factors beyond the timing of single events (for instance, the recurrence of AGN activity) play a role in shaping the cosmic evolution of the bulk AGN population.

To investigate this, we model the occurrence times of AGN events as independently and identically distributed, making two key assumptions: (1) the occurrence time follows a single distribution in each episode, and (2) the occurrence time for each individual AGN is independent of others, with no direct influence on the timing of subsequent events. Under these assumptions, we generate a set of independent random variables t_i , drawn from a log-normal distribution to represent individual AGN occurrence times. We then compute the probability distribution of the total elapsed time across multiple episodes, defined as the sum of n independent

¹ Although the fitting result generally depends on the choice of time bin, the consistency of the fitted parameters based on the differential and cumulative distribution functions ensures the robustness of the fitting result.

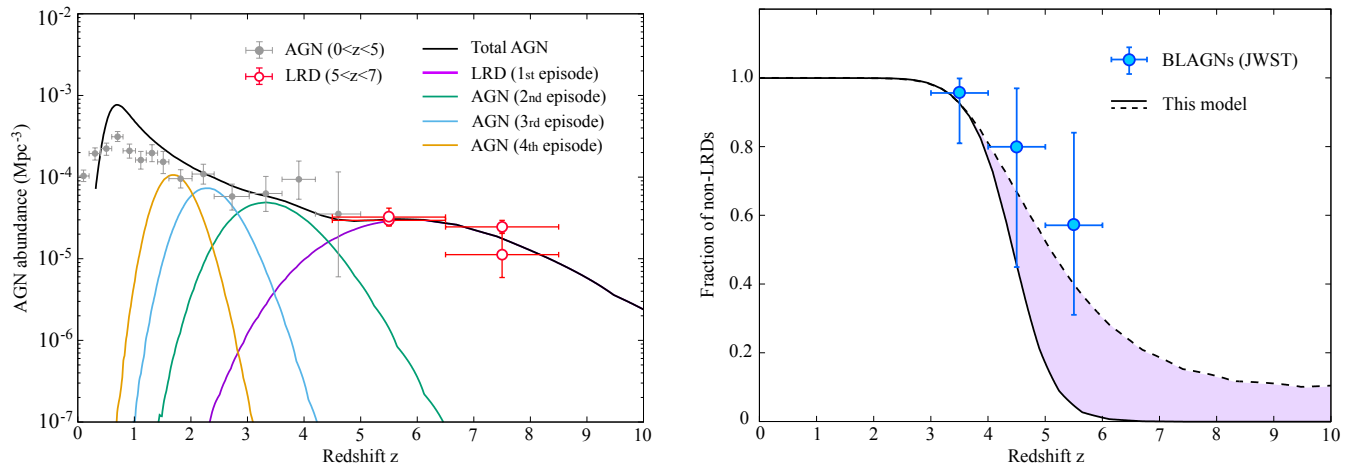


Figure 2. *Left:* The redshift dependence of the AGN comoving number density. Each modeled curve presents the AGN population that undergo n -th AGN active episodes, illustrating the distribution of the total elapsed time T_n ($1 \leq n \leq 8$): the first (magenta), second (green), third (cyan), fourth (orange) episodes, as well as the total population in this model (black). The normalization is set such that the modeled LRD abundance is consistent with the observed ones (red symbols, Kokorev et al. 2024; Kocevski et al. 2024). The total AGN predicted in this model agrees with measurements of AGN abundances in the range $0 < z < 5$ (gray symbols, Ueda et al. 2014). *Right:* The fraction of non-LRDs (black solid; model) and observational constraints on the fraction (95% confidence level) derived from a sample of 53 broad-line AGNs (blue symbol, Taylor et al. 2024). The shaded region indicates the range of uncertainty due to the choice of the absolute time origin for the LRD occurrence distribution.

log-normal variables, $T_n = \sum_{i=1}^n t_i$. To obtain a statistically robust distribution, we perform Monte Carlo sampling for each T_n and numerically construct its probability distribution. Note that as $n \rightarrow \infty$, the distribution of T_n approaches a Gaussian distribution according to the central limit theorem, allowing for an analytical treatment for this calculation (see Appendix C).

In the left panel of Figure 2, each curve presents the AGN population categorized by the number of active episodes that the nuclear BH undergo, showing the distribution of T_n : the first ($n = 1$; magenta), second ($n = 2$; green), third ($n = 3$; cyan), fourth ($n = 4$; orange) episodes, as well as the total population, which includes up to eight episodes ($n = 8$; black). The normalization of the modeled abundance is set such that the number of objects in their first active episodes matches the observed abundance of LRDs at $z \sim 4 - 7$, which is $\phi_{\text{LRD}} \simeq 3 \times 10^{-5} \text{ Mpc}^{-3}$ (Kocevski et al. 2024; Akins et al. 2024; Kokorev et al. 2024). Since the total number of objects is conserved across successive episodes, the modeled AGN abundance at $z < 5$ is not explicitly fitted to the observational data over $0 < z < 5$ (gray symbols; Ueda et al. 2014). Although the LRD number decreases at $z < 4$, the total AGN abundance curve increases toward lower redshifts, reflecting the shift from LRDs to more typical AGN populations. This trend is consistent with our finding of $\phi \propto (1 + z)^{-5/2}$, which is derived from the nearly constant occurrence rate of AGN activity (see Equation C3).

In the right panel of Figure 2, we show the fraction of AGNs that have experienced their second or later episodes relative to the total AGN population, representing the fraction of non-LRDs under this hypothesis. Since a significant fraction of BHs undergo a second episode at $z < 5$, this fraction increases rapidly and reaches unity by $z \sim 3$. For comparison, we overlay observational constraints on the fraction of unobscured (non-LRD) AGNs (95% confidence level), derived from a sample of 53 spectroscopically confirmed broad-line AGNs in the redshift range of $3.5 < z < 6$ (Taylor et al. 2024). At $z \leq 6$, the sample size in each redshift bin is sufficiently large to reveal a trend that closely follows the model prediction (black solid)².

One key uncertainty in this model is the absolute time origin for the LRD occurrence times. The first LRDs should emerge following a log-normal distribution, only after their parent dark-matter halos virialize, the baryonic components condense via radiative cooling, and BHs form. To account for this, we introduce a temporal shift of ΔT , with a maximum value of 500 Myr, corresponding to the cosmic time when the most distant LRDs are observed. The right panel of Figure 2 represents this adjusted model, where the interval between

² Since the sample size at $6 < z < 7$ is too small for robust statistical analysis (one LRD and two unobscured AGNs), we do not include the data in the right panel of Figure 2. Statistical uncertainties are evaluated using the Clopper-Pearson method.

individual AGN episodes is shortened by $\Delta T = 500$ Myr (dashed curve), and the possible range of variations within $0 \leq \Delta T \leq 500$ Myr (shaded region). The redshift range where LRDs begin to diminish coincides with the emergence of typical unobscured AGNs.

The emergence conditions of LRDs are likely tied to the underlying BH seeding mechanisms and surrounding environment. One proposed model is the heavy seed scenario, in which seed BHs form through the direct collapse of massive atomic gas clouds (e.g., Loeb & Rasio 1994; Bromm & Loeb 2003; Begelman et al. 2006; Shang et al. 2010, see also Inayoshi et al. 2020). Alternatively, the lack of an obvious host galaxy component in LRDs (Chen et al. 2024) implies that processes beyond baryonic physics might be involved. For instance, the collapse of a halo core via energy dissipation in a self-interacting dark matter environment has been proposed (e.g., Feng et al. 2021; Grant Roberts et al. 2025). In both scenarios, a key prediction is that BH formation precedes active star formation. Moreover, the initial accretion episodes onto newly-born seed BHs are likely led by intense cold flows along cosmic filaments in overdense regions of the universe (Di Matteo et al. 2012) and may occur through gas with low angular momentum (Eisenstein & Loeb 1995). The timing of these accretion processes, potentially influenced by the spin distribution of the halo, may be crucial for the emergence of LRDs.

The physical origin of the log-normal occurrence distribution for LRDs (and more broadly, AGN activity) remains an open question. However, the observed statis-

tical properties suggest that the occurrence time, t_{AGN} , is determined by the product of multiple independent physical quantities x_i ($i = 1, 2, \dots, n$) with some inherent randomness, such that

$$t_{\text{AGN}} = x_1 x_2 \cdots x_n. \quad (2)$$

If the logarithms of these variables, $\log x_i$, follow distributions that satisfy weak conditions, the central limit theorem implies that the distribution of $\log t_{\text{AGN}}$ tends toward a normal distribution as n increases. In astrophysical contexts, while $n \rightarrow \infty$ is not strictly applicable, even a modest number ($n \sim 3$) is sufficient to produce a log-normal distribution (e.g., Ioka & Nakamura 2002). This statistical (i.e., *macroscopic*) property can be described without specifying the detailed *microscopic* physical processes that govern AGN triggering. Modeling the specific mechanisms that set the mean and variance of the distribution will be left for future studies.

ACKNOWLEDGMENTS

I greatly thank Changhao Chen, Kejian Chen, Zoltán Haiman, Luis C. Ho, Kenta Hotokezaka, Kohei Ichikawa, Dale D. Kocevski, Masafusa Onoue, and Jinyi Shang-guan for constructive discussions. I acknowledge support from the National Natural Science Foundation of China (12073003, 11721303, 11991052), and the China Manned Space Project (CMS-CSST-2021-A04 and CMS-CSST-2021-A06).

APPENDIX

A. SELECTION

The left panel of Figure 3 shows the distribution of LRD detections as a function of absolute UV magnitude with the total sample (purple) and subsets at $z \geq 6$ (green), $z \geq 7$ (blue), and $z \geq 8$ (orange). The histogram peaks at $M_{\text{UV}} \sim -18$ mag with a decline on both the brighter and fainter sides. The rarity of LRDs on the brighter end suggests an intrinsically lower abundance, while the decline on the fainter end is likely due to flux limits, as also seen in the UV luminosity functions at $M_{\text{UV}} > -18$ mag (Kocevski et al. 2024). The characteristic bending magnitude remains consistent across all redshift bins.

The right panel of Figure 3 presents the LRD occurrence rate for each UV-magnitude bin, along with the best-fit log-normal distribution (solid curves). The fitted parameters, summarized in Table 2, fall within the 1σ uncertainty range. Even when considering only bright LRDs with $M_{\text{UV}} < -18$ mag, the emergence trend of LRDs at $t \gtrsim 0.5$ Gyr remains robust. Thus, we conclude that this trend reflects an intrinsic phenomenon rather than a selection effect.

B. DIMINISHING LRD FEATURES DUE TO MERGERS WITH OTHER GALAXIES

One possible explanation for the decline in the LRD occurrence rate at $z < 4 - 5$ is that their unique features, especially their compact morphology (e.g., Labbe et al. 2023; Kocevski et al. 2024), are lost due to mergers with normal galaxies. Major mergers could cause LRDs to appear as extended sources, blending stellar components with the underlying AGN and diminishing their LRD-like characteristics. Indeed, dual LRD candidates with $\sim 1 - 2$ kpc projected separations have been reported (Tanaka et al. 2024). Cosmological N -body simulations estimate that major

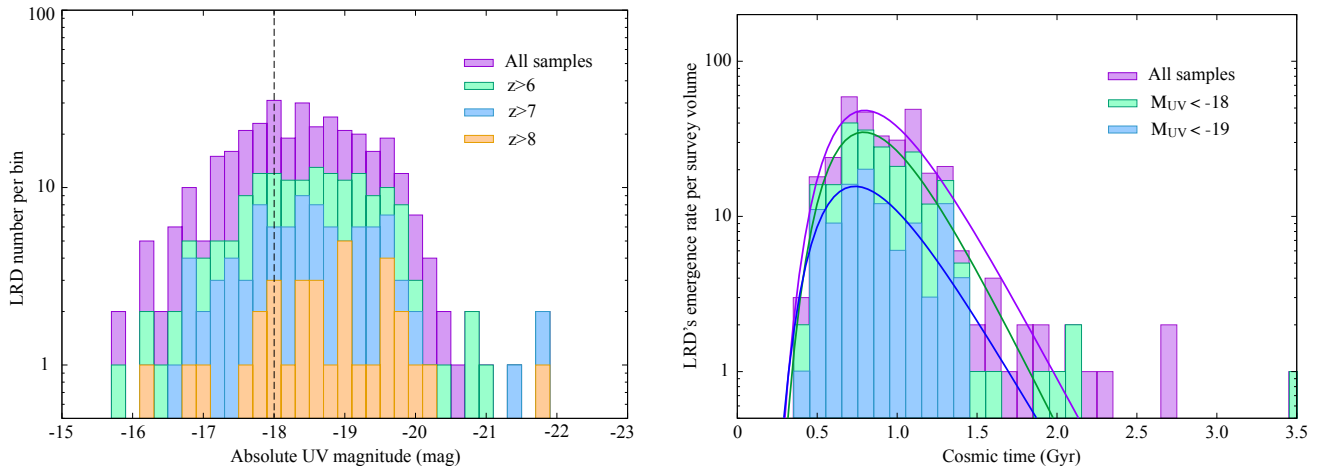


Figure 3. *Left:* The distribution of UV absolute magnitudes for LRDs with the total sample (purple) and subsets at $z \geq 6$ (green), $z \geq 7$ (blue), and $z \geq 8$ (orange). The vertical line indicates a reference threshold of $M_{UV} = -18$ mag, fainter than which the observed decline in number is likely due to flux limits. *Right:* The LRD occurrence rate for the total sample (purple) and subsets at $M_{UV} < -18$ (green) and $M_{UV} < -19$ (blue) overlaid with best-fit log-normal distributions (solid curves).

Table 2. Fitting results with a log-normal distribution.

(1)	(2)	(3)
	t_0 (Myr)	σ_0
All sample	888 ± 30	0.326 ± 0.0341
$M_{UV} < -18$	869 ± 20	0.319 ± 0.0259
$M_{UV} < -19$	833 ± 38	0.357 ± 0.0502

mergers (with a mass ratio of $\xi \gtrsim 0.3$) occur with a frequency of $p \sim 0.2$ per halo per redshift interval (Fakhouri et al. 2010). This suggests that the number of LRDs that avoid such mergers and retain their unique features decreases toward lower redshifts as

$$\frac{dN_{\text{LRD}}}{dz} \simeq N_0 e^{-p(z_0 - z)}. \quad (\text{B1})$$

Figure 4 presents two curves representing dN_{LRD}/dt for $p = 0.2$ (cyan) and $p = 0.5$ (blue), where N_0 is adjusted to match the histogram at a cosmic age of ~ 1 Gyr. The case with $p = 0.2$ approximately corresponds to a scenario where the comoving number density of LRDs follows a power-law evolution, $\phi \propto t^{-1}$, consistent with the overall cosmic evolution of the number density of galaxies over $0 < z < 8$ (Conselice et al. 2016). Even in an extreme case where $p = 0.5$ (implying that 50% of LRDs undergo merger in each redshift interval, a rate observed in simulations for minor mergers), the resulting decline trend is still significantly shallower than the log-normal decay (magenta curve). This suggests that mergers alone cannot fully account for the rapid disappearance of LRDs at lower redshifts, unless minor mergers with $\xi \gtrsim 0.03$ would diminish LRD characteristics.

C. ANALYTIC FORMULA

When the occurrence times of AGN events are independently and identically distributed, the central limit theorem states that the cumulative occurrence time until the n -th AGN event will approximately follow a Gaussian distribution with mean $n\mu$ and variance $n\sigma^2$, where μ and σ^2 are the mean and variance of the occurrence time distribution for each single event. Although the occurrence timing follows a log-normal distribution, for simplicity, we approximate it as a Gaussian distribution with mean μ and variance σ^2 . This assumption allows for an analytical treatment for the

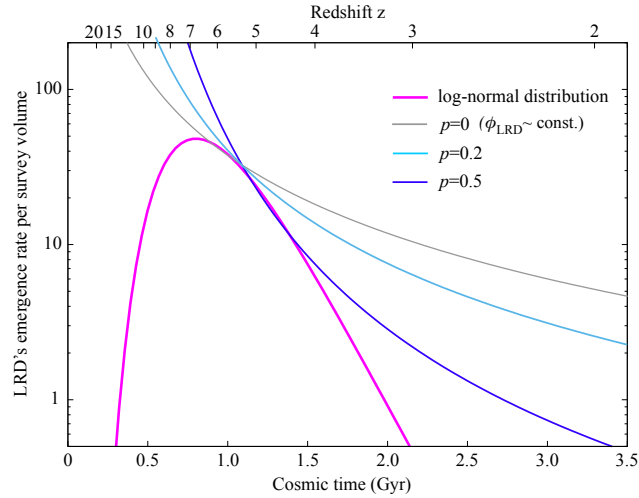


Figure 4. The LRD occurrence-rate models: the log-normal case (magenta) and the decay cases driven by mergers: $p = 0$ (gray), $p = 0.2$ (cyan), and $p = 0.5$ (blue).

calculation of the cosmic AGN occurrence rate. The total occurrence rate at a given cosmic time t is expressed as

$$\frac{dN_{\text{AGN}}}{dt} = \sum_{k=1}^n \frac{N_0}{\sqrt{2\pi}\sigma_k} e^{-(t-\mu_k)^2/2\sigma_k^2}, \quad (\text{C2})$$

where $\mu_k = k\mu$ and $\sigma_k = \sqrt{k}\sigma$ for $1 \leq k \leq n$. For sufficiently large $k \gtrsim k_0 \equiv (\mu/\sigma)^2$, the dispersion σ_k becomes large enough that the separation between each Gaussian peak becomes smaller than the dispersion, and thus each Gaussian distribution largely overlaps. Therefore, at later times of $t > k_0\mu = \mu^3/\sigma^2$, the sum can be approximated by an integral form and evaluated using the saddle-point method around $x = t/\mu$,

$$\frac{dN_{\text{AGN}}}{dt} = \frac{N_0}{\sqrt{2\pi}\sigma} \int_0^\infty \exp\left[\frac{-(t-\mu x)^2}{2\sigma^2 x}\right] \frac{dx}{x} \simeq \frac{N_0}{\mu}. \quad (\text{C3})$$

The result turns out *time-independent*. This trend is consistent with the numerical result of $\phi \propto (1+z)^{-5/2}$ shown in Figure 2, and aligns with measurements of AGN abundances in the range $0 < z < 5$ (Ueda et al. 2014) as well.

REFERENCES

- Akins, H. B., Casey, C. M., Lambrides, E., et al. 2024, arXiv e-prints, arXiv:2406.10341, doi: [10.48550/arXiv.2406.10341](https://doi.org/10.48550/arXiv.2406.10341)
- Begelman, M. C., Volonteri, M., & Rees, M. J. 2006, MNRAS, 370, 289, doi: [10.1111/j.1365-2966.2006.10467.x](https://doi.org/10.1111/j.1365-2966.2006.10467.x)
- Bromm, V., & Loeb, A. 2003, ApJ, 596, 34, doi: [10.1086/377529](https://doi.org/10.1086/377529)
- Chen, C.-H., Ho, L. C., Li, R., & Zhuang, M.-Y. 2024, arXiv e-prints, arXiv:2411.04446, doi: [10.48550/arXiv.2411.04446](https://doi.org/10.48550/arXiv.2411.04446)
- Conselice, C. J., Wilkinson, A., Duncan, K., & Mortlock, A. 2016, ApJ, 830, 83, doi: [10.3847/0004-637X/830/2/83](https://doi.org/10.3847/0004-637X/830/2/83)
- Delvecchio, I., Gruppioni, C., Pozzi, F., et al. 2014, MNRAS, 439, 2736, doi: [10.1093/mnras/stu130](https://doi.org/10.1093/mnras/stu130)
- Di Matteo, T., Khandai, N., DeGraf, C., et al. 2012, ApJL, 745, L29, doi: [10.1088/2041-8205/745/2/L29](https://doi.org/10.1088/2041-8205/745/2/L29)
- Eisenstein, D. J., & Loeb, A. 1995, ApJ, 443, 11, doi: [10.1086/175498](https://doi.org/10.1086/175498)
- Ellsworth, W. L., Matthews, M. V., Nadeau, R. M., et al. 1999, A physically-based earthquake recurrence model for estimation of long-term earthquake probabilities, Tech. rep., US Geological Survey
- Fakhouri, O., Ma, C.-P., & Boylan-Kolchin, M. 2010, MNRAS, 406, 2267, doi: [10.1111/j.1365-2966.2010.16859.x](https://doi.org/10.1111/j.1365-2966.2010.16859.x)
- Feng, W.-X., Yu, H.-B., & Zhong, Y.-M. 2021, ApJL, 914, L26, doi: [10.3847/2041-8213/ac04b0](https://doi.org/10.3847/2041-8213/ac04b0)
- Grant Roberts, M., Braff, L., Garg, A., et al. 2025, JCAP, 2025, 060, doi: [10.1088/1475-7516/2025/01/060](https://doi.org/10.1088/1475-7516/2025/01/060)

- Greene, J. E., Labbe, I., Goulding, A. D., et al. 2024, *ApJ*, 964, 39, doi: [10.3847/1538-4357/ad1e5f](https://doi.org/10.3847/1538-4357/ad1e5f)
- Hainline, K. N., Maiolino, R., Juodžbalis, I., et al. 2025, *ApJ*, 979, 138, doi: [10.3847/1538-4357/ad9920](https://doi.org/10.3847/1538-4357/ad9920)
- Harikane, Y., Zhang, Y., Nakajima, K., et al. 2023, *ApJ*, 959, 39, doi: [10.3847/1538-4357/ad029e](https://doi.org/10.3847/1538-4357/ad029e)
- Hu, H., Inayoshi, K., Haiman, Z., et al. 2022, *ApJ*, 935, 140, doi: [10.3847/1538-4357/ac7daa](https://doi.org/10.3847/1538-4357/ac7daa)
- Inayoshi, K., Kimura, S., & Noda, H. 2024, arXiv e-prints, arXiv:2412.03653, doi: [10.48550/arXiv.2412.03653](https://doi.org/10.48550/arXiv.2412.03653)
- Inayoshi, K., Nakatani, R., Toyouchi, D., et al. 2022, *ApJ*, 927, 237, doi: [10.3847/1538-4357/ac4751](https://doi.org/10.3847/1538-4357/ac4751)
- Inayoshi, K., Visbal, E., & Haiman, Z. 2020, *ARA&A*, 58, 27, doi: [10.1146/annurev-astro-120419-014455](https://doi.org/10.1146/annurev-astro-120419-014455)
- Ioka, K., & Nakamura, T. 2002, *ApJL*, 570, L21, doi: [10.1086/340815](https://doi.org/10.1086/340815)
- Ji, X., Maiolino, R., Übler, H., et al. 2025, arXiv e-prints, arXiv:2501.13082, doi: [10.48550/arXiv.2501.13082](https://doi.org/10.48550/arXiv.2501.13082)
- Juodžbalis, I., Ji, X., Maiolino, R., et al. 2024, arXiv e-prints, arXiv:2407.08643, doi: [10.48550/arXiv.2407.08643](https://doi.org/10.48550/arXiv.2407.08643)
- Kirsten, F., Ould-Boukattine, O. S., Herrmann, W., et al. 2024, *Nature Astronomy*, 8, 337, doi: [10.1038/s41550-023-02153-z](https://doi.org/10.1038/s41550-023-02153-z)
- Kocevski, D. D., Onoue, M., Inayoshi, K., et al. 2023, *ApJL*, 954, L4, doi: [10.3847/2041-8213/ace5a0](https://doi.org/10.3847/2041-8213/ace5a0)
- Kocevski, D. D., Finkelstein, S. L., Barro, G., et al. 2024, arXiv e-prints, arXiv:2404.03576, doi: [10.48550/arXiv.2404.03576](https://doi.org/10.48550/arXiv.2404.03576)
- Kokorev, V., Caputi, K. I., Greene, J. E., et al. 2024, *ApJ*, 968, 38, doi: [10.3847/1538-4357/ad4265](https://doi.org/10.3847/1538-4357/ad4265)
- Kormendy, J., & Ho, L. C. 2013, *ARA&A*, 51, 511, doi: [10.1146/annurev-astro-082708-101811](https://doi.org/10.1146/annurev-astro-082708-101811)
- Labbe, I., Greene, J. E., Bezanson, R., et al. 2023, arXiv e-prints, arXiv:2306.07320, doi: [10.48550/arXiv.2306.07320](https://doi.org/10.48550/arXiv.2306.07320)
- Li, H., & Fenimore, E. E. 1996, *ApJL*, 469, L115, doi: [10.1086/310275](https://doi.org/10.1086/310275)
- Li, W., Inayoshi, K., Onoue, M., & Toyouchi, D. 2023, *ApJ*, 950, 85, doi: [10.3847/1538-4357/acbbbe](https://doi.org/10.3847/1538-4357/acbbbe)
- Li, W., Inayoshi, K., & Qiu, Y. 2021, *ApJ*, 917, 60, doi: [10.3847/1538-4357/ac0adc](https://doi.org/10.3847/1538-4357/ac0adc)
- Loeb, A., & Rasio, F. A. 1994, *ApJ*, 432, 52, doi: [10.1086/174548](https://doi.org/10.1086/174548)
- Madau, P., & Haardt, F. 2024, arXiv e-prints, arXiv:2410.00417, doi: [10.48550/arXiv.2410.00417](https://doi.org/10.48550/arXiv.2410.00417)
- Maiolino, R., Scholtz, J., Curtis-Lake, E., et al. 2023, arXiv e-prints, arXiv:2308.01230, doi: [10.48550/arXiv.2308.01230](https://doi.org/10.48550/arXiv.2308.01230)
- Maiolino, R., Risaliti, G., Signorini, M., et al. 2024, arXiv e-prints, arXiv:2405.00504, doi: [10.48550/arXiv.2405.00504](https://doi.org/10.48550/arXiv.2405.00504)
- Matthee, J., Naidu, R. P., Brammer, G., et al. 2024, *ApJ*, 963, 129, doi: [10.3847/1538-4357/ad2345](https://doi.org/10.3847/1538-4357/ad2345)
- Onoue, M., Inayoshi, K., Ding, X., et al. 2023, *ApJL*, 942, L17, doi: [10.3847/2041-8213/aca9d3](https://doi.org/10.3847/2041-8213/aca9d3)
- Pérez-González, P. G., Barro, G., Rieke, G. H., et al. 2024, arXiv e-prints, arXiv:2401.08782, doi: [10.48550/arXiv.2401.08782](https://doi.org/10.48550/arXiv.2401.08782)
- Pouliasis, E., Ruiz, A., Georgantopoulos, I., et al. 2024, arXiv e-prints, arXiv:2401.13515, doi: [10.48550/arXiv.2401.13515](https://doi.org/10.48550/arXiv.2401.13515)
- Reines, A. E., & Volonteri, M. 2015, *ApJ*, 813, 82, doi: [10.1088/0004-637X/813/2/82](https://doi.org/10.1088/0004-637X/813/2/82)
- Scoggins, M. T., & Haiman, Z. 2024, *MNRAS*, 531, 4584, doi: [10.1093/mnras/stae1449](https://doi.org/10.1093/mnras/stae1449)
- Shang, C., Bryan, G. L., & Haiman, Z. 2010, *MNRAS*, 402, 1249, doi: [10.1111/j.1365-2966.2009.15960.x](https://doi.org/10.1111/j.1365-2966.2009.15960.x)
- Tanaka, T. S., Silverman, J. D., Shimasaku, K., et al. 2024, arXiv e-prints, arXiv:2412.14246, doi: [10.48550/arXiv.2412.14246](https://doi.org/10.48550/arXiv.2412.14246)
- Taylor, A. J., Finkelstein, S. L., Kocevski, D. D., et al. 2024, arXiv e-prints, arXiv:2409.06772, doi: [10.48550/arXiv.2409.06772](https://doi.org/10.48550/arXiv.2409.06772)
- Trinca, A., Schneider, R., Valiante, R., et al. 2022, *MNRAS*, 511, 616, doi: [10.1093/mnras/stac062](https://doi.org/10.1093/mnras/stac062)
- Ueda, Y., Akiyama, M., Hasinger, G., Miyaji, T., & Watson, M. G. 2014, *ApJ*, 786, 104, doi: [10.1088/0004-637X/786/2/104](https://doi.org/10.1088/0004-637X/786/2/104)
- Valiante, R., Schneider, R., Volonteri, M., & Omukai, K. 2016, *MNRAS*, 457, 3356, doi: [10.1093/mnras/stw225](https://doi.org/10.1093/mnras/stw225)
- Volonteri, M., Habouzit, M., & Colpi, M. 2021, *Nature Reviews Physics*, 3, 732, doi: [10.1038/s42254-021-00364-9](https://doi.org/10.1038/s42254-021-00364-9)
- Wang, B., de Graaff, A., Davies, R. L., et al. 2024a, arXiv e-prints, arXiv:2403.02304, doi: [10.48550/arXiv.2403.02304](https://doi.org/10.48550/arXiv.2403.02304)
- Wang, B., Leja, J., de Graaff, A., et al. 2024b, *ApJL*, 969, L13, doi: [10.3847/2041-8213/ad55f7](https://doi.org/10.3847/2041-8213/ad55f7)